

## Supporting Information

### **Near-infrared-triggered antibacterial and antifungal photodynamic therapy based on lanthanide-doped upconversion nanoparticles**

Yuxiang Zhang,<sup>abc</sup> Ping Huang,<sup>ac</sup> Dong Wang,<sup>ac</sup> Jincan Chen,<sup>a</sup> Wenzhen Liu,<sup>ac</sup> Ping Hu,<sup>a</sup>  
Mingdong Huang,<sup>a</sup> Xueyuan Chen,<sup>\*ac</sup> and Zhuo Chen<sup>\*ac</sup>

<sup>a</sup> State Key Laboratory of Structural Chemistry, CAS Key Laboratory of Design and Assembly of Functional Nanostructures, and Fujian Key Laboratory of Nanomaterials, Fujian Institute of Research on the Structure of Matter, Chinese Academy of Sciences, Fuzhou, Fujian 350002, China.

<sup>b</sup> Fujian Agriculture and Forestry University, Fuzhou, Fujian 350002, China.

<sup>c</sup> University of Chinese Academy of Sciences, Beijing 100049, China.

E-mail: [xchen@fjirsm.ac.cn](mailto:xchen@fjirsm.ac.cn) or [zchen@fjirsm.ac.cn](mailto:zchen@fjirsm.ac.cn); Fax: + 86 591 63179421; Tel: +86 591 63173094

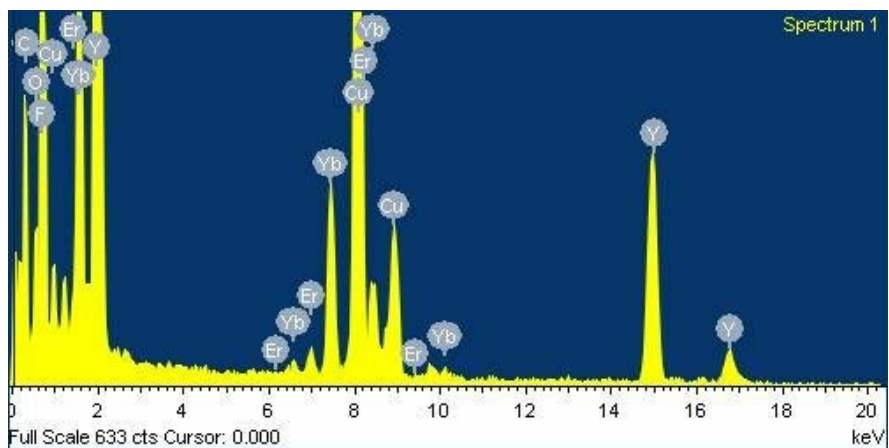


**Figure S1.** EDX analysis of  $\text{LiYF}_4:\text{Yb/Er}$  NPs, revealing the presence of Y, F and doped Yb, Er elements in  $\text{LiYF}_4$  host.

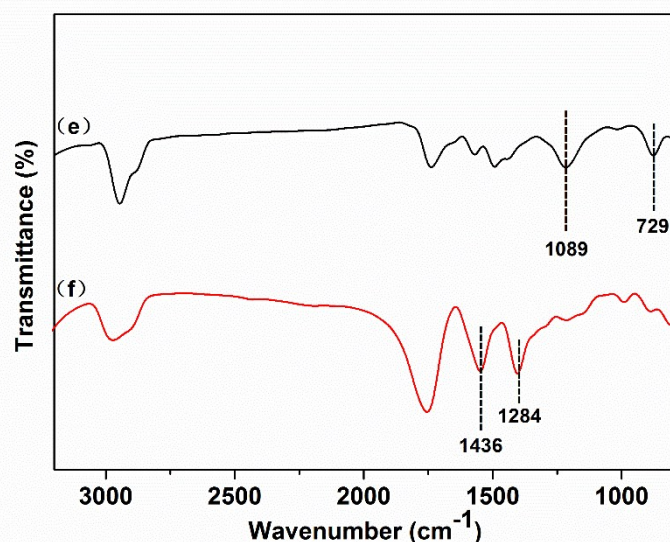
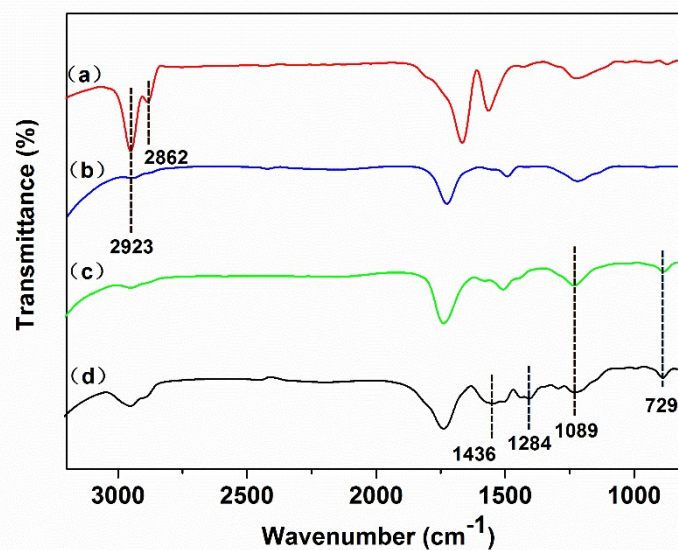


**Figure S2.** Fourier transform infrared (FTIR) spectra of (a) oleate-capped UCNPs, (b) ligand-free UCNPs, (c) UCNPs-CPZ, (d) UCNPs-CPZ-PVP, (e) CPZ and (f) PVP. The intensities of the original asymmetric and symmetric stretching vibrations of methylene ( $-\text{CH}_2-$ ) in the long alkyl chain peaking at 2923 and 2862  $\text{cm}^{-1}$  in the ligand-free UCNPs were markedly weakened, reconfirming the successful removal of oleate ligands from the surface of oleate-capped UCNPs. Two IR bands centered at 1089 and 729  $\text{cm}^{-1}$  were observed for UCNPs-CPZ, which were attributed to the stretching vibrations of the phthalocyanine aromatic ring and the C-H groups on the phthalocyanine aromatic ring of CPZ. Besides, two bands were also observed at 1436 and 1284  $\text{cm}^{-1}$  for UCNPs-CPZ-PVP, which were attributed to the vibrations of the C—N bond and C—H bond of PVP.

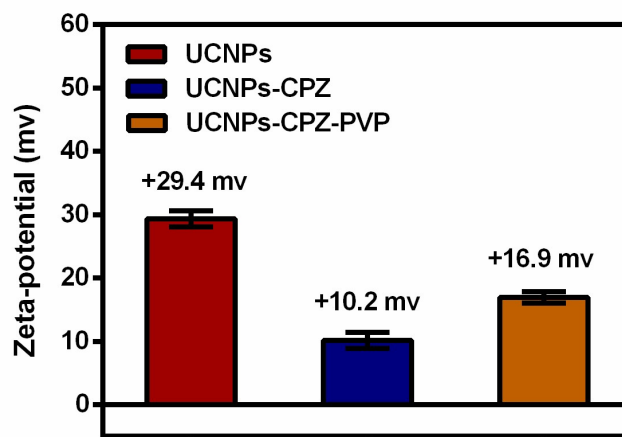


**Figure S3.**  $\zeta$ -potentials of the ligand-free UCNPs, UCNPs-CPZ and UCNPs-CPZ-PVP obtained from DLS measurement at pH 6.5. After loading CPZ, the  $\zeta$ -potentials of UCNPs changed from +29.4 to +10.2 mV, suggesting a successful conjugation of CPZ to UCNPs.  $\zeta$ -potentials was subsequently increased (+16.9 mV) after coating with PVP, indicating the successful decoration of PVP to the surface of UCNPs-CPZ.

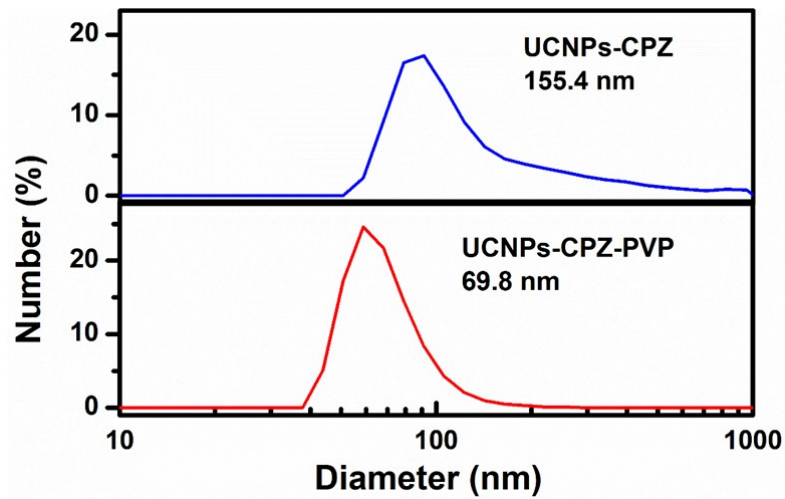


**Figure S4.** Comparison of the hydrodynamic diameter distributions between UCNPs-CPZ and UCNPs-CPZ-PVP in 0.9% saline solution. Compared with UCNPs-CPZ, UCNPs-CPZ-PVP exhibited an obvious reduced distribution of hydrodynamic diameter (69.8 nm), indicating that PVP was an appropriate agent to prevent the aggregation of UCNPs-CPZ.

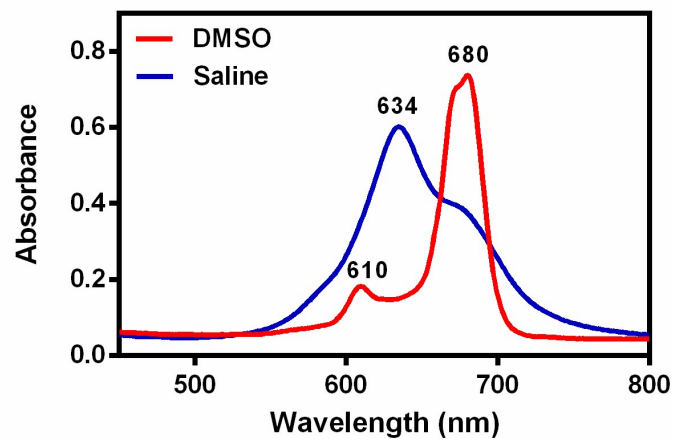


**Figure S5.** Absorption spectra of CPZ either in DMSO or in a mixed solution containing 1% DMSO and 0.9% saline. A characteristic absorption peak at 680 nm of CPZ (in DMSO) represented the monomer state of CPZ, while the peak of CPZ shifted from 680 nm to 634 nm in a mixed solution containing 1% DMSO and 0.9% saline, indicating the aggregation of CPZ.

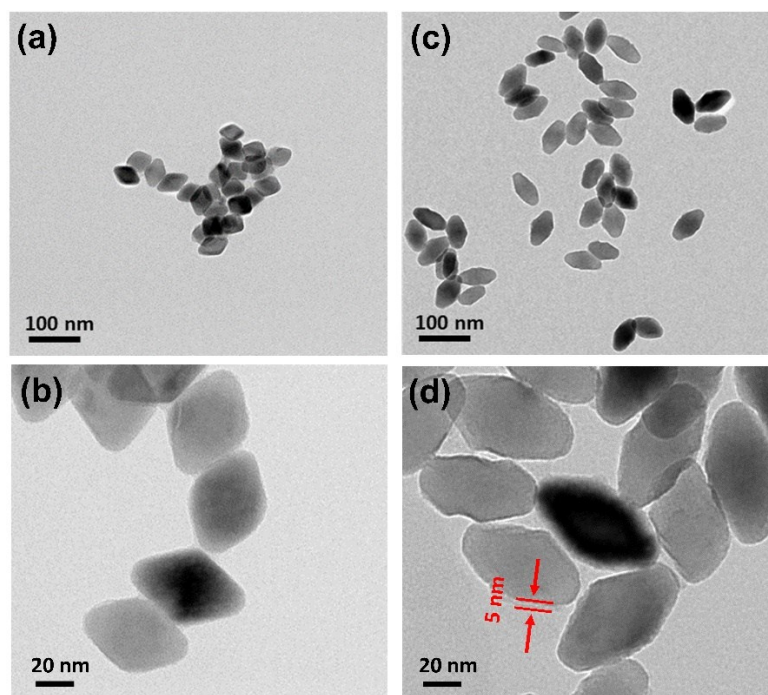


**Figure S6.** TEM images of (a, b) UCNPs-CPZ and (c, d) UCNPs-CPZ-PVP. By calculating 200 particles in the TEM images, the mean size of the nanocomposites was determined to increase from  $(57 \pm 4) \times (40 \pm 3)$  nm for UCNPs-CPZ to  $(67 \pm 6) \times (41 \pm 5)$  nm for UCNPs-CPZ-PVP, as a result of PVP coating. A discernible contrasted core/shell nanostructure can be explicitly observed in UCNPs-CPZ-PVP. The brighter region marked in Fig. S6d shows a PVP layer with a thickness of 5 nm.

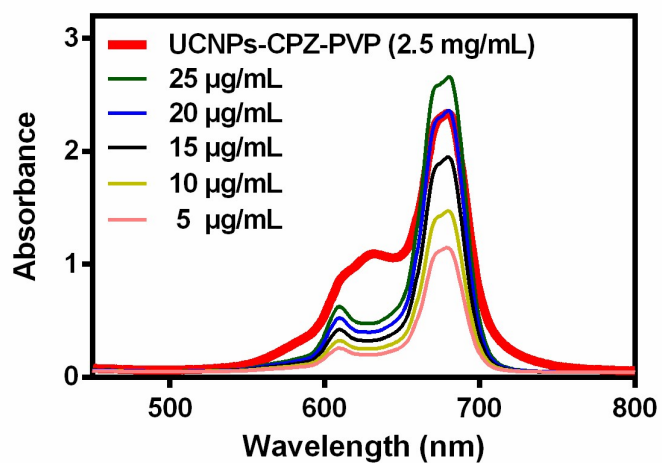


**Figure S7.** Absorption spectra of CPZ (at concentrations of 5, 10, 15, 20 and 25 µg/mL, respectively) and the UCNPs-CPZ-PVP (2.5 mg/mL) in DMSO. The loading amount of CPZ was determined to be about 0.8 % (w/w) on the UCNPs-CPZ-PVP.

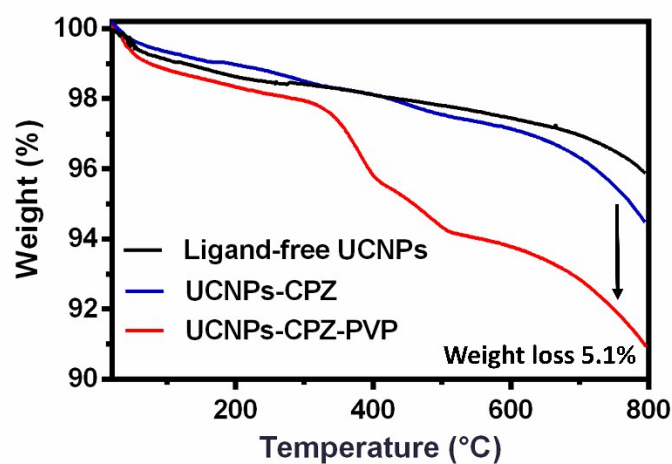


**Figure S8.** Thermogravimetric analyses (TGA) curves of ligand-free  $\text{LiYbF}_4:\text{Yb}/\text{Er}$  UCNPs, UCNPs-CPZ and UCNPs-CPZ-PVP under  $\text{N}_2$  atmosphere in the temperature range of 20-800 °C at a rate of 10 °C/min. Different decomposition temperatures and weight losses were observed, due to different ligands capped on the surface of UCNPs. By comparing the weight losses between UCNPs-CPZ and UCNPs-CPZ-PVP, the content of PVP coated on UCNPs-CPZ-PVP was quantified to be 5.1 % (w/w).

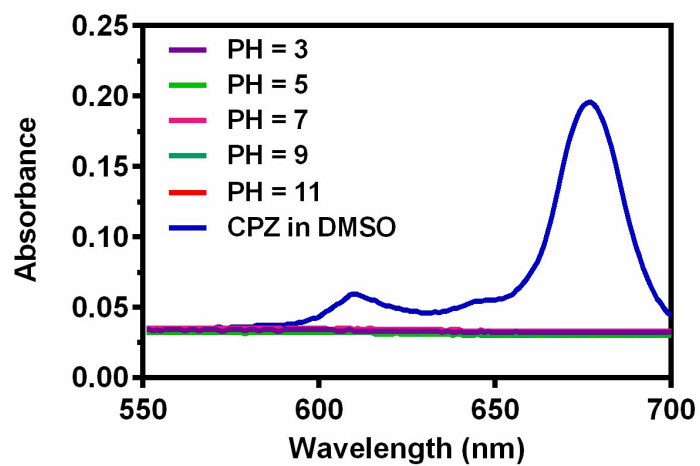


**Figure S9.** Stability testing of the UCNPs-CPZ-PVP nanocomposites in 0.9% saline solution with different pH values (ranging from 3 to 11). No release of CPZ was detected after 48-h observation of the UCNPs-CPZ-PVP, suggesting a high stability of UCNPs-CPZ-PVP.

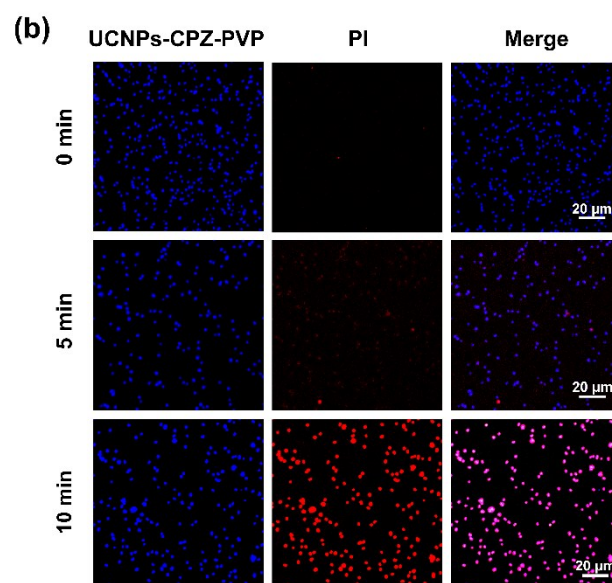
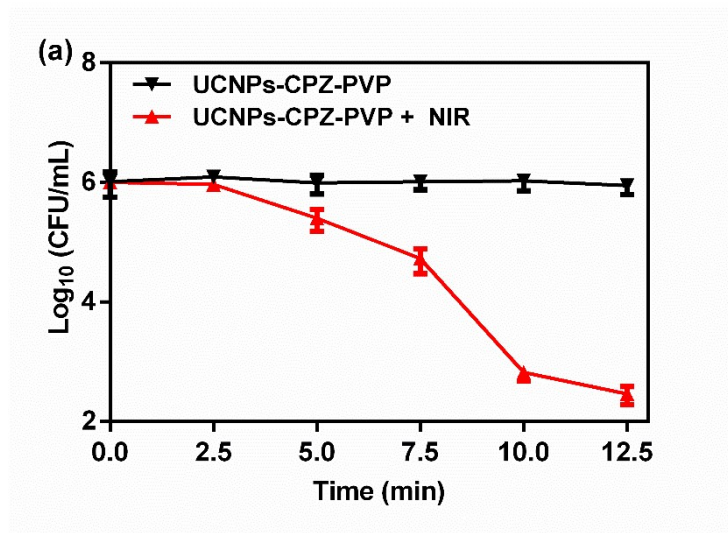


**Figure S10.** Antibacterial effects of 980-nm irradiation time period ( $0.5 \text{ W/cm}^2$ ) on MRSA after a 30-min incubation with the UCNPs-CPZ-PVP ( $30 \mu\text{g/mL}$ ). (a) Viability of MRSA after aPDT with different time periods of irradiation (0, 2.5, 5, 7.5, 10 and 12.5 min). (b) CLSM images of MRSA after aPDT with different time periods of irradiation (0, 5 and 10 min). Scale bar was  $20 \mu\text{m}$ .

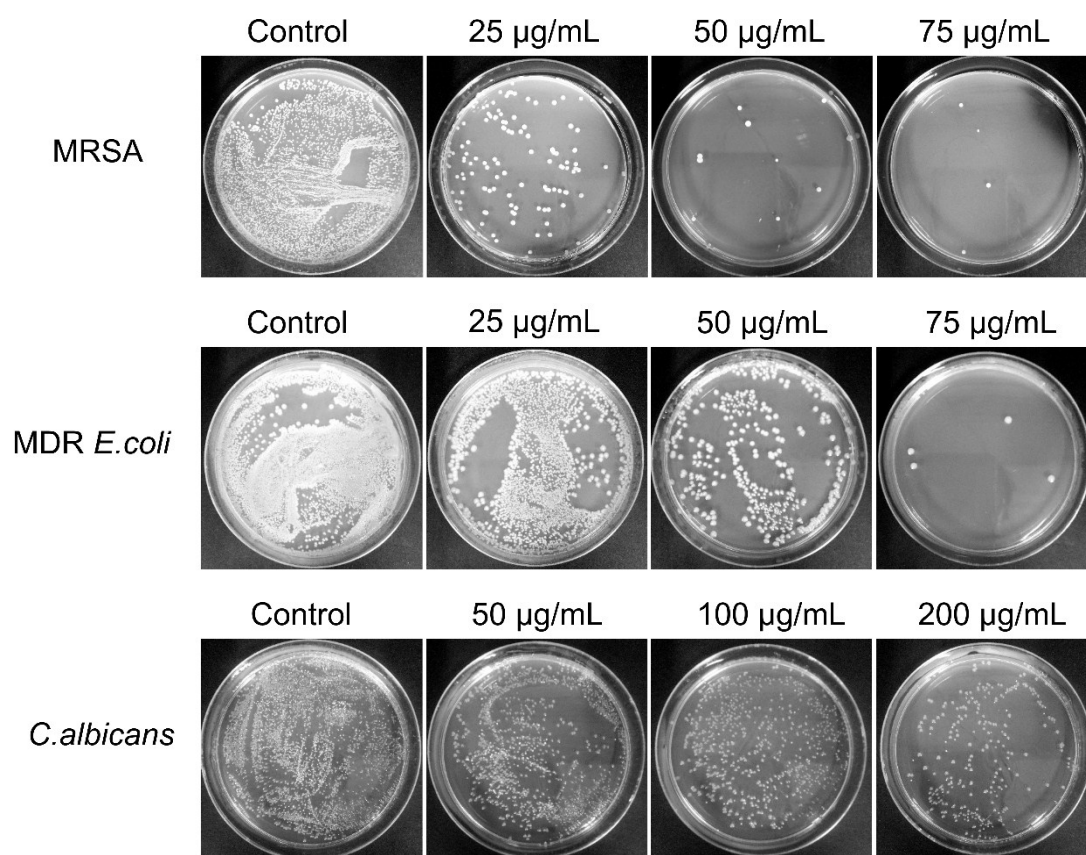


**Figure S11.** Estimation of microbial numbers of MRSA, MDR *E. coli* and *C. albicans* by CFU counting method after aPDT with UCNPs-CPZ-PVP (at concentrations of 0, 25, 50 and 75  $\mu\text{g/mL}$ , respectively) upon 980 nm laser irradiation.

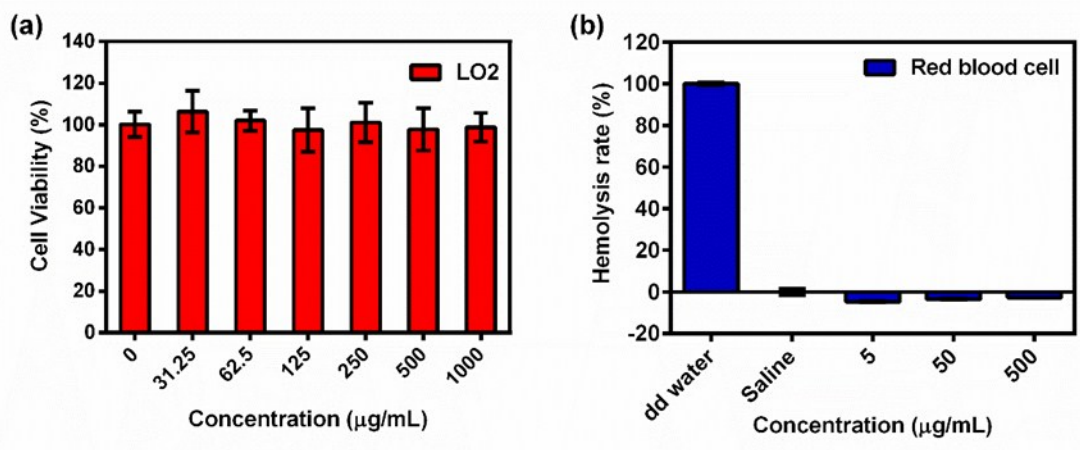


**Figure S12.** Biosafety of the UCNPs-CPZ-PVP nanocomposites. The LO2 cell compatibility (a) and the blood compatibility (b) experiments disclosed a good biological compatibility of the UCNPs-CPZ-PVP.